Spectroscopic and molecular docking studies on the interaction of human serum albumin with copper(II) complexes

Bhargab Guhathakurta, Ankur Bikash Pradhan, Suman Das, Nirmalya Bandyopadhyay, Liping Lu, Miaoli Zhu, Jnan Prakash Naskar

PII: S1386-1425(16)30638-2
DOI: doi:10.1016/j.saa.2016.10.043
Reference: SAA 14742

To appear in:

Received date: 15 July 2016
Revised date: 20 October 2016
Accepted date: 21 October 2016

Please cite this article as: Bhargab Guhathakurta, Ankur Bikash Pradhan, Suman Das, Nirmalya Bandyopadhyay, Liping Lu, Miaoli Zhu, Jnan Prakash Naskar, Spectroscopic and molecular docking studies on the interaction of human serum albumin with copper(II) complexes, (2016), doi:10.1016/j.saa.2016.10.043

Spectroscopic and molecular docking studies on the interaction of human serum albumin with copper(II) complexes

Bhargab Guhathakurta[a], Ankur Bikash Pradhan[a], Suman Das[a], Nirmalya Bandyopadhyay[a], Liping Lu[b], Miaoli Zhu[b], Jnan Prakash Naskar[a,*]

[a]*Department of Chemistry, Jadavpur University, Kolkata-700 032, India. Fax: +(91)(33)2414 6223 E-mail: jpnaskar@rediffmail.com*

[b]*Institute of Molecular Science, Key Laboratory of Chemical Biology and Molecular Engineering of the Education Ministry, Shanxi University, 92 Wucheng Road, Taiyuan, Shanxi- 030006, People's Republic of China.*

Abstract

Two osazone based ligands, butane-2,3-dione bis(2′-pyridylhydrazone) (BDBPH) and hexane-3,4-dione bis(2′-pyridylhydrazone) (HDBPH), were synthesized out of the 2:1 molar Schiff base condensation of 2-hydrazino pyridine respectively with 2,3-butanedione and 3,4-hexanedione. The X-ray crystal structures of both the ligands have been determined. The copper(II) complex of HDBPH has also been synthesized and structurally characterized. HDBPH and its copper(II) complex have thoroughly been characterized through various spectroscopic and analytical techniques. The X-ray crystal structure of the copper complex of HDBPH shows that it is a monomeric Cu(II) complex having 'N_4O_2' co-ordination chromophore. Interaction of human serum albumin (HSA) with these ligands and their monomeric copper(II) complexes have been studied by various spectroscopic means. The experimental findings show that the ligands as well as their copper complexes are good HSA binders. Molecular docking investigations have also been done to unravel the mode of binding of the species with HSA.

Key words: Osazone, Copper, Crystal structure, HSA binding, Molecular docking

1. Introduction

In 1964, B. Chiswell and F. Lions reported metal complexes of an osazone based ligand, butane-2,3-dione bis(2′-pyridylhydrazone). This planar quadridentate chelating agent was generated through the condensation of biacetyl and 2-hydrazino pyridine [1]. α-Dicarbonyl precursors like glyoxal, biacetyl and cyclohexane-1,2-dione are prone to yield osazones on treatment with 2-hydrazino pyridine. On the contrary, α-diketones like benzil, phenanthraquinone, acenaphthenequinone are averse to form osazones so much so that they react with 2-hydrazino pyridine to give rise only the mono-(2-pyridylhydrazone) [2]. Osazone of benzil and 2-hydrazino pyridine was first synthesized by F. H. Case and co-workers [3]. Osazones are analytical chromogenic reagents. Butane-2,3-dione bis(2′-pyridylhydrazone) (BDBPH/$\mathbf{L^1H_2}$) is a known colorimetric reagent, often used for the determination of Co(II) and Pd(II) ions [2,4,5]. Osazones obtained from hydrazine/substituted hydrazine may or may not undergo protonic dissociation of the two dissociable NH protons during the course of their metal binding. For ready reckoning, BDBPH binds to copper(II) in protonated form [6]; while to nickel(II) only after its deprotonation [7]. The crystal structure of bare BDBPH is, however, not known till date. The structure of the monomeric copper(II) complex of BDBPH, as determined by us, reveals that the compound crystallizes in the monoclinic space group [6]. This one-electron paramagnetic copper(II) complex is in Jahn-Teller distorted octahedral geometry. The copper center resides in a 'N_4O_2' coordination chromophore.

The most abundant protein in human blood plasma is human serum albumin (HSA). HSA executes a plethora of crucial physiological functions aided by its enhanced solubility in blood plasma. It regulates osmotic blood pressure and helps in the storage, transportation, metabolism and distribution of biologically important compounds. HSA acts as the disposer of different exogenous and endogenous species through plasma circulation. Again, it deactivates radicals and delivers amino acids after hydrolysis for the synthesis of new

proteins [8]. HSA plays an indispensible ubiquitous role in circulatory system to maintain blood pH level [9]. Besides, HSA anchors and transports metal ions, fatty acids, hormones, steroids, vitamins and a variety of pharmaceuticals including metal based drugs efficiently with minimal toxicity. Thus, HSA has relevance in molecular pharmacology and pharmacokinetics as well. HSA also reduces the chance of the oxidation of the bound drug [10]. Tumour cells take up and accumulate HSA at an enhanced level in comparison to their normal counterparts. Accordingly, HSA offers the efficacy to serve as carrier conjugate of antimalignant drugs like paclitaxel and doxorubicin [11]. HSA is significant from clinical oncological viewpoint too. Owing to these versatile yet benign myriad prospects, studies on the binding of HSA encompass a burgeoning area of contemporary research in chemical biology and pharmacology [12]. Again, from the pharmacological and toxicological view-point the metal complexes show significant advantages over the organic compounds [13,14]. Metal complexes facilitate the transport processes through cell membranes and protect the drug from enzymatic degradation [15]. Copper, a bio essential trace element, is notable in this perspective. Copper complexes play a crucial role in different biological processes like electron transfer, DNA damage and as anticancer agents [16]. These aspects kindled our interest to undertake the studies on the interaction of copper(II) complexes derived from osazone based ligands, $\mathbf{L^1H_2}$ and $\mathbf{L^2H_2}$ and to evaluate their subsequent HSA binding prospects.

Here we wish to report the syntheses, characterization and structures of a novel ligand, hexane-3,4-dione bis (2′-pyridylhydrazone) (HDBPH/$\mathbf{L^2H_2}$) and its copper(II) complex, $CuL^2H_2(ClO_4)_2.H_2O$ (**2**). The crystal structure of another analogous ligand system $\mathbf{L^1H_2}$ butane-2,3-dione bis(2′-pyridylhydrazone) has also been determined. Syntheses of $\mathbf{L^1H_2}$ and its copper(II) complex, $CuL^1H_2(ClO_4)_2$ (**1**) have been reported previously by us [6]. The HSA

binding and molecular docking aspects of the above ligands and their copper(II) complexes have also been dealt with.

2. Experimental

2.1. Materials and measurements

All chemicals were of analytical reagent grade and were used as received without further purification. 2,3-butanedione, 3,4-hexanedione and 2-hydrazino pyridine were procured from Aldrich, USA. HSA was purchased from Sigma-Aldrich Corporation (St. Louis, MO, USA). Electro-thermal digital melting point apparatus (SUMSIM India) was employed for determining the melting point of the ligand and it is uncorrected. C, H and N microanalyses were done on a Perkin-Elmer 2400II elemental analyzer. Copper was estimated gravimetrically as its white CuSCN complex. FT-IR spectra (KBr disc) [(vb) = very broad, (b) = broad, (m) = medium, (s) = strong] of $\mathbf{L^2H_2}$ and **2** were recorded employing a Nicolet Magna-IR spectrophotometer (Series II). UV-Vis spectra (in MeOH) of $\mathbf{L^2H_2}$ and **2** were recorded on a Shimadzu UV-160A spectrophotometer. A Bruker DPX300 MHz spectrometer was used to run the ^{1}H NMR spectrum (in $CDCl_3$: reference, TMS) of $\mathbf{L^2H_2}$. ESI mass spectra of both $\mathbf{L^2H_2}$ and **2** were recorded on a Waters Q-TOF Micro YA263 spectrometer in methanol. Electric conductivity measurements of **2** were performed at room temperature on a Systronics (India) direct reading conductivity meter (model 304). A PAR 155 vibrating sample magnetometer fitted with a walker scientific L75FBAL magnet, calibrated with $Hg[Co(SCN)_4]$, was used to determine the magnetic susceptibility of **2** at room temperature. The magnetic susceptibility data were corrected for diamagnetism using Pascal's constants.

Caution: Perchlorate salts of metal complexes can be explosive [17]. Although no detonation tendencies have been observed, care is advised and handling of only small quantity is recommended.

2.2. Buffer and protein solutions

Using the molar absorption coefficient value of 42 864 M^{-1} cm^{-1} at 280 nm [18], the concentration of HSA solution was determined. 10 mM citrate-phosphate (CP) buffer of pH 7.0 was used to perform all the experiments. The CP buffer solution was made in quartz-distilled deionized water from a Milli-Q source (Millipore, USA). Then the solution was filtered to remove impurities with Millipore filters of 0.45 μm pore size.

The mother solutions of the ligands as well as their copper complexes were prepared in water-methanol (4:1) mixed solvent. We chose this mixed solvent for the necessary inclusion of CP buffer in the milieu to undertake the protein binding study under physiological conditions. To check the stability of the ligands and their copper complexes in this mixed solvent, we have taken the UV-Vis spectra of the ligands and their complexes maintaining the physiological pH. The spectra of the ligands and their complexes correlate nicely with their respective spectra, taken only in pure methanol, in terms of band positions with expected features.

2.3.Methods for HSA Binding

2.3.1. UV−Visible Spectroscopy

Shimadzu (model UV-1800) spectrophotometer (Shimadzu Corporation, Japan) was used to measure all the UV−Vis absorption spectra. Matched quartz cuvettes having 1 cm path length were used throughout the study. During the experiment, a thermoprogrammer was attached to the spectrophotometer via Peltier effect to maintain the temperatures of the sample and reference cuvettes. Keeping the sample concentration fixed at 4.9 μM and with the rising concentration of HSA until the saturation point is reached, the spectrophotometric titrations were performed. At the λ_{max} value, the changes in the absorption spectra were noted for each sample until saturation was obtained.

2.3.2. Spectrofluorimetric studies

Shimadzu RF-5301PC spectrofluorimeter (Shimadzu Corporation, Kyoto, Japan) was used to analyse the steady-state fluorescence spectral data for the samples. Free quartz cell of 1 cm path length was used to record the fluorescence data. The excitation and emission bandpass were respectively of 3 and 5 nm. A fixed amount of ligands as well as complexes (9.2 μM) was titrated with increasing concentration of HSA at the same excited λ_{max} of 285 nm.

2.3.3. Fluorescence lifetime measurements

In the absence and in the presence of rising concentration of HSA in 10 mM CP buffer of pH 7.0 at 25 °C for the fluorescence decay of the samples, time correlated single photon counting (TCSPC) measurements were done. The photoexcitation was performed at 300 nm using a picosecond diode laser (IBH Nanoled-07) in an IBH fluorocube apparatus. Using IBH DAS6 software [from the equation (1)], fluorescence decay data were analysed which were collected on a Hamamatsu MCP photomultiplier (R3809).

$$F(t) = \sum_i \alpha_i e(-\frac{t}{\tau}) \qquad (1)$$

Here α_i represents the ith pre-exponential factor and τ stands for the decay time. The lifetime of the excited species is referred to as decay time.

2.3.4. *Thermodynamic studies: temperature dependent spectrofluorometry*

Temperature dependent emission spectra were recorded in a Horiba-Jobin-Yvon Fluoromax-4 spectrofluorimeter attached with thermometric cell temperature programmer and temperature controller. These measurements were performed at 15, 25 and 35 °C.

The values of K′ were determined at different temperatures. Thermodynamic parameters were estimated by analysis of van't Hoff plot (ln K′ versus 1/T) obtained over the temperature range of the study. The slope of the plot gives the binding enthalpy change (ΔH^0) as

$$\partial \ln(K') / \partial(1/T) = -\frac{\Delta H^o}{R} \qquad (2)$$

The Gibbs free energy change (ΔG^0) was determined from the binding constant at a particular temperature according to this relation

$$\Delta G^0 = -RT \ln(K') \qquad (3)$$

The entropy change (ΔS^0) was then estimated from the following equation

$$\Delta S^0 = \left(\Delta H^0 - \Delta G^0 / T\right) \qquad (4)$$

2.4. Molecular docking studies

AutoDock (version 4.2) was used to find out the binding interaction and the probable binding sites of ligands as well as complexes with HSA. The X-ray crystal structure of HSA was taken from RCS Protein Data Bank having PDB code 1AO6. 3D structure of the four samples was created in Chem3D Ultra 8.0. Using two well-known software packages Gaussian 09W and AutoDock 4.2, necessary modification was done. The DFT//B3LYP/6-31G level of theory was used to optimize the geometry of the samples using the Gaussian 09W set and the Gauss view 5.0 software in a compatible file format was used to exploit the optimized geometry and to generate the required file in AutoDock 4.2. Polar hydrogen atoms and Gasteiger charges were added to the protein and ligand/complex. To perform the docking simulations, a grid box with dimensions of 120, 120 and 120 Å and a grid spacing of 0.403 Å were assigned. Other parameters were taken as usual as the default values set by the AutoDock program. AutoGrid was used to deliberate the grid maps for energy and the docking calculations were done by Lamarckian genetic algorithm (LGA). The best optimized docked model having lowest energy was chosen for further analysis of docking simulations which was best viewed in PyMOL and Mercury software.

2.5. Synthesis of ligands and complexes

2.5.1. Preparation of Ligand, BDBPH ($\mathbf{L^1H_2}$)

The synthesis and general characterization of $\mathbf{L^1H_2}$ was reported in our previous communication [6].

Needle-shaped yellow single crystals of $\mathbf{L^1H_2}$, fit for X-ray crystallography, were grown during the course of slow evaporation of a moderately concentrated solution of it in methanol.

2.5.2 Preparation of Ligand, HDBPH ($\boldsymbol{L^2H_2}$)

0.03 mL (0.25 mmol) of 3,4-hexanedione was dissolved in 15 mL of dry methanol. Then 0.56 mg (0.51 mmol) of 2-hydrazinopyridine was added to it all at a time. The resulting yellow orange mixture was refluxed under heating for 4 h. After refluxing, the resulting yellow solution was kept in a refrigerator for slow evaporation. After 10 days, the separated ligand was filtered and was washed with ice-cold diethyl ether thoroughly. The ligand is soluble in methanol, acetonitrile and chloroform but insoluble in benzene, petroleum ether, diethyl ether and water. Yield: 48 mg (64%), m. p.: 216-220 °C. $C_{16}H_{20}N_6$ (296.16): Anal. Calc. for $C_{16}H_{20}N_6$: C, 64.83; H, 6.81; N, 28.36. Found: C, 64.96; H, 6.76; N, 28.42 %. FT-IR (KBr) ν/cm^{-1}: 3197vb (NH), 1676vb (C=N imine), 1598, 1575, 1436s (aromatic C=C ring vibration frequencies), 1575b (amine), 987m (pyridine ring), 773s (four adjacent H on aromatic ring) and 738m (mono-substituted pyridine). UV-Vis (MeOH): λ_{max} ($\varepsilon/M^{-1}\ cm^{-1}$) 273 (11 240), 292 (37 810) and 329 (39 680). ^{1}H NMR ($CDCl_3$): δ/ppm 8.32 (2H, s, –NH– proton), 8.13 (2H, d, *o*-proton of pyridine ring), 7.59 (2H, t, *p*-proton of pyridine ring), 7.32 (2H, d, *m*-proton of pyridine ring near –NH– group), 6.79 (2H, t, *m*-proton of pyridine ring), 3.48 (4H, t, ethyl protons), 2.17 (6H, d, ethyl protons). ESI-MS (positive ion mode) (*m/z*): 297.1304 (calcd. 297.3781) for $[L^2H_2+H^+]$ (100%), 295.1235 (calcd. 295.2908) for $[L^2H_2–2H^{\cdot}+H^+]$ (30%) and 319.1163 (calcd. 319.3599) for $[L^2H_2+Na^+]$ (50%). We got yellow needle-shaped single crystals of $\mathbf{L^2H_2}$, suitable for X-ray crystal structure determination, by slow aerial evaporation of the mother liquor of $\mathbf{L^2H_2}$ in methanol.

*2.5.3. Preparation of $CuL^1H_2(ClO_4)_2$ (**1**)*

The preparation and thorough characterization of **1** was reported earlier by us [6].

*2.5.4. Preparation of $CuL^2H_2(ClO_4)_2.H_2O$ (**2**)*

12 mg (0.04 mmol) of **L^2H_2** was dissolved in 15 mL of MeOH. Then 15 mg (0.04 mmol) of solid $Cu(ClO_4)_2.6H_2O$ was added all at a time with constant stirring to the yellow ligand solution. The colour of the solution changed to brick red almost instantly. The resulting red reaction mixture was stirred for 2 h. After stirring, the resulting solution was kept in a refrigerator for slow evaporation. After 7 days, the separated dark red compound was filtered and washed with ice-cold diethyl ether thoroughly. Then it was dried in a vacuum desiccator over fused $CaCl_2$. The compound is soluble in methanol, acetonitrile and acetone but insoluble in benzene, petroleum ether, diethyl ether, dichloromethane and water.

Yield: 16 mg (66%). $C_{16}H_{22}N_6CuO_9Cl_2$ (576.67): Anal. Calc. for $C_{16}H_{22}N_6CuO_9Cl_2$: C, 33.29; H, 3.84; N, 14.57; Cu, 11.01; Found C, 33.21; H, 3.75; N, 14.71; Cu, 10.92%. FT-IR (KBr): v 3414vb (OH), 1614s (C=N of imine), 1485s (C=N of oxime), 1230s (N-O), 1113vs (ClO_4) and 631s (ClO_4) cm^{-1}. UV-Vis (MeOH): λ_{max} (ε/M^{-1} cm^{-1}) 273 (1 502), 338 (6 078), 366 (6 850) and 446 (1 136) ESI-MS (positive ion mode) (*m/z*): 358.0315 (calcd. 358.3623) for $[Cu^{63}(L^2H_2)–2H^+ + H^+]$ (100%), 360.0375 (calcd. 360.3623) for $[Cu^{65}(L^2H_2)–2H^+ + H^+]$ (40%) and 357.0356 (calcd. 357.3543) for $[Cu^{63}(L^2H_2)–H^{\cdot}–H^+]$ (30%). Λ_M (MeOH): 207.37 $cm^2ohm^{-1}mol^{-1}$ (1:2 electrolyte), Λ_M (MeCN): 235.23 $cm^2ohm^{-1}mol^{-1}$ (1:2 electrolyte). μ_{eff}/μ_B: 1.94 (at 298 K).

We got needle-shaped red single crystals of this compound fit for X-ray structure determination by slow evaporation of the moderately concentrated solution of the compound in acetone on standing in a refrigerator.

2.6. Crystal structure determination

Single crystals suitable for X-ray crystallographic analyses were selected after examination under a microscope. A Bruker Smart APEX II diffractometer equipped with 1K charge-coupled device (CCD) area detector and graphite monochromated MoKα radiation (λ =

0.71073 Å) was used for the data collection of $\mathbf{L^1H_2}$, $\mathbf{L^2H_2}$ and $\mathbf{CuL^2H_2(ClO_4)_2.H_2O}$ respectively at 273, 298 and 100 K. The cell parameters were determined using SMART software [19]. SAINTPlus [19] was used for data reduction and correction. Absorption corrections were made by SADBAS [20]. The structures were solved by direct methods with SHELXL-97 program [21] and also were refined by full-matrix least-squares methods on all F^2 data by SHELXL-97. The anisotropic refinement was done over all non-hydrogen atoms. Subsequently, the additional H-atoms were placed at their respective parent atoms and also were refined using riding model. Lastly, the cycle of full-matrix least-squares refinement was made on the basis of observed reflections and variable parameters. All structural refinement values of $\mathbf{L^1H_2}$, $\mathbf{L^2H_2}$ and $\mathbf{CuL^2H_2(ClO_4)_2.H_2O}$ are given in Table 1. Some selected bond lengths, bond angles and hydrogen-bond geometries of them are tabulated respectively in Tables 2 and 3. The cif files of $\mathbf{L^1H_2}$, $\mathbf{L^2H_2}$ and **2** were deposited with the Cambridge Crystallographic Data Centre (CCDC) bearing CCDC Nos. 1446043, 1446044 and 1446045 respectively.

3. Results and discussion

3.1. Synthesis and formulation

$\mathbf{L^1H_2}$ is the di-condensate Schiff base adduct of diacetyl with 2-hydrazino pyridine. $\mathbf{L^2H_2}$, an analogous osazone of $\mathbf{L^1H_2}$, is derived from 3,4-hexanedione with 2-hydrazino pyridine. They are obtained in copious yields out of the reaction of respective diketone with 2-hydrazino pyridine in 1:2 stoichiometric proportions in dehydrated methanol (Scheme. 1).

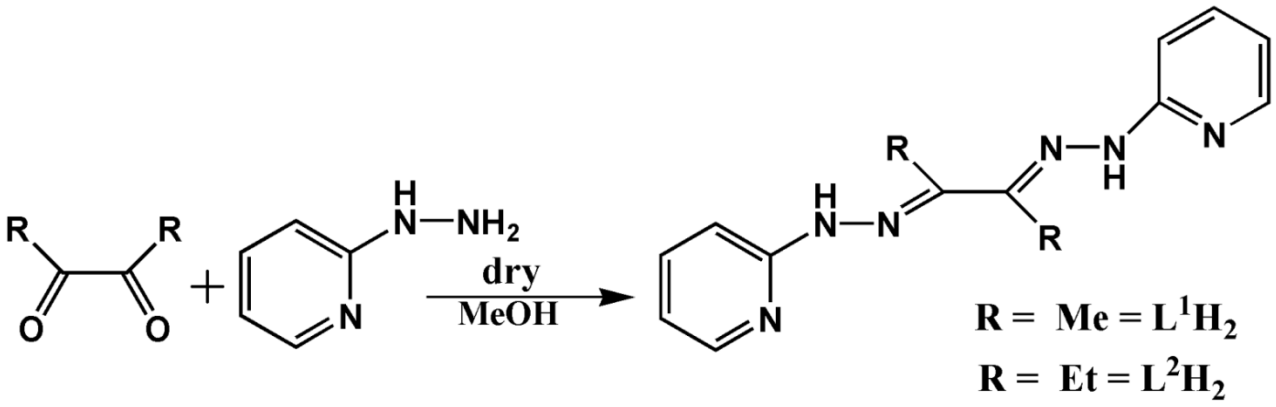

Scheme. 1. Synthetic scheme of the ligands

Our subsequent reaction of $\mathbf{L^1H_2}$ and $\mathbf{L^2H_2}$ with copper(II)perchlorate hexahydrate in 1:1 stoichiometric proportion in methanol at room temperature yielded monomeric copper(II) complexes, **1** and **2**, with moderate yields. Preparation of $\mathbf{L^1H_2}$ and **1** had been reported earlier by us. Both **1** and **2** are air stable for indefinite period. In the IR spectrum of $\mathbf{L^2H_2}$ a new bond stretching frequency is observed at 1676 cm^{-1} which is indicative of (C=N imine) bond. This is indicative of the formation of Schiff base [22]. At 1113 cm^{-1} a broad double split band is observed in the IR spectrum of **2**. This is assigned to the coordinated perchlorate with the copper center [23]. The ESI-MS mass spectra of $\mathbf{L^2H_2}$ and **2** show the presence of two dissociable protons on the ligand skeleton. This feature is akin to the earlier work on this class of ligand [7].

3.2. Crystal structures of L^1H_2, L^2H_2 and **2**

$\mathbf{L^1H_2}$ crystallizes in the monoclinic crystal system having space group P2(1)/c, with z value of 2. Centrosymmetric $\mathbf{L^2H_2}$ also crystallizes in the monoclinic space group, C2/c, with four molecular weight units accommodated per unit cell. The C-N bonds are found to be 1.2880 [N3–C6] and 1.284 Å [C1–N1] respectively for $\mathbf{L^1H_2}$ and $\mathbf{L^2H_2}$. These values are almost similar. The corresponding N–N bond distances in $\mathbf{L^1H_2}$ and $\mathbf{L^2H_2}$ are found to be 1.3002 and 1.3654 Å. Both the ligands exist in stereochemical *anti* conformational preference over their *cis* disposition to get rid of steric strain. The crystal structures of $\mathbf{L^1H_2}$ and $\mathbf{L^2H_2}$ are shown

respectively in Fig. 1 and Fig. 2. The crystal structure of **2** (Fig. 3) reveals that the copper centre of this mononuclear copper(II) complex is in 'N_4O_2' octahedral coordination environment. The tetradentate ligand, $\mathbf{L^2H_2}$ provides four nitrogen donor centers [two pyridyl nitrogen donors, N1 and N6; two nitrogen donors from the hydrazine residue, N3 and N4]. The two oxygen donors from the coordinating perchlorate, O1 and O5, complete the 'N_4O_2' core. The Cu1–N3, Cu1–N4, Cu1–N6 and Cu1–N1 bond distances are respectively of 1.9577(12), 1.9585(12), 1.9913(12) and 1.9953(11) Å. Accordingly, they are of the same order of magnitude. On the contrary, the two axial bonds, Cu1–O1 and Cu1–O5. are respectively of 2.5753(13) and 2.5456(13) Å. These data are similar with that reported previously for other mononuclear octahedral Cu(II) complex [24].The axial bond lengths are of higher magnitude as expected in Jahn-Teller distorted octahedral copper(II) system. This axial elongation is the natural consequence of an octahedral copper(II) complex [6].

Table1

Crystal data and structure refinement for $\mathbf{L^1H_2}$, $\mathbf{L^2H_2}$ and **2**

	$\mathbf{L^1H_2}$	$\mathbf{L^2H_2}$	**2**
CCDC No.	1446043	1446044	1446045
Empirical formula	$C_{14}H_{16}N_6$	$C_{16}H_{20}N_6$	$C_{16}H_{22}Cl_2CuN_6O_9$
Formula weight	268.33	296.38	576.83
Temperature [K]	273(2)	298(2)	100(2)
Wavelength [Å]	0.71073	0.71073	0.71073
Crystal system	Monoclinic	Monoclinic	Monoclinic
Space group	P2(1)/c	C2/c	P2(1)/c
Unit cell dimensions			
a [Å]	8.8092(4)	13.3888(6)	8.0850(16)
b [Å]	4.7855(2)	13.9584(6)	10.191(2)

c [Å]	16.1183(8)	8.9084(3)	26.913(5)
β [^{o}]	94.457(4)	100.667(3)	95.79(3)
Volume [Å^3]	677.44(5)	1636.09(12)	2206.2(8)
Absorption coefficient [mm^{-1}]	0.085	0.077	1.295
Absorption correction	multi-scan	multi-scan	multi-scan
Z	2	4	4
ρ_{Calcd} [g/cm^3]	1.315	1.203	1.737
F(000)	284	632	1180
Crystal size [mm]	0.21×0.06×0.04	0.24×0.07×0.05	0.29×0.05×0.07
Reflections collected	9159	11694	10523
Parameters	92	101	309
R_1, all data, R_1 [$I > 2\sigma$(I)]	0.0422,0.1104	0.0433,0.1207	0.0379,0.1196
$wR_{2,\text{all data}}$, wR_2 [$I > 2\sigma$(I)]	0.0535,0.1169	0.0524,0.1304	0.0389,0.1213
*S*onF^2	1.076	1.033	1.034
Largest diff. peak	0.148	0.201	0.491
Largest diff. hole [eÅ^{-3}]	-0.179	-0.156	-0.919

Table2

Selected bond distances (Å) and angles (º)

For **L^{1}H$_2$**

N1–C1	1.3333(19)	C1–C2	1.391(2)
N1–C5	1.341(2)	C2–C3	1.364(2)
N2–N3	1.3628(17)	C3–C4	1.372(2)
N2–C1	1.3785(19)	C4–C5	1.361(3)

N3–C6	1.2880(18)	C6–C7	1.488(2)
C6–C6#1	1.470(3)	C2–H2	0.9300
C1–N1–C5	116.55(14)	N3–N2–C1	118.10(12)
C6–N3–N2	118.67(12)	C3–C2–C1	118.41(15)
N1–C1–N2	115.34(13)	N1–C1–C2	122.72(14)
N2–C1–C2	121.94(14)		

For $\mathbf{L^2H_2}$

N1–C1	1.284(2)	C1–C2	1.503(2)
N1–N2	1.3654(16)	C2–C3	1.492(3)
N2–C4	1.3777(19)	N3–C4	1.3279(18)
N3–C8	1.345(2)	C4–C5	1.389(2)
C6–C7	1.372(3)	C7–C8	1.360(3)
C1–C1#2	1.475(3)	N2–H2	0.8600
C1–N1–N2	119.40(13)	N1–N2–C4	117.02(12)
C4–N3–C8	116.67(14)	N1–C1–C1#1	114.85(17)
N1–C1–C2	125.77(13)	C1#1–C1–C2	119.32(17)
C3–C2–C1	112.47(17)	N3–C4–N2	114.90(13)

For **2**

Cu1–N3	1.9577(12)	Cu1–N4	1.9585(12)
Cu1–N6	1.9913(12)	Cu1–N1	1.9953(11)
Cu1–O1	2.5753(13)	Cu1–O5	2.5456(13)
N1–C1	1.3454(17)	N1–C5	1.3558(18)
N2–N3	1.3002(18)	N4–C7	1.2999(17)
N3–N5	1.3516(15)	N5–C12	1.3883(17)
N6–C12	1.3500(17)	N6–C16	1.3570(17)

Cl1–O4	1.4402(11)	Cl1–O1	1.4662(11)
O1–Cu1–N3	91.67(5)	N1–C1–C2	122.51(12)
O1–Cu1–N4	86.70(5)	C3–C2–C1	118.49(13)
N3–Cu1–N4	78.74(5)	N2–C5–C4	120.80(13)
O1–Cu1–N1	92.33(5)	N1–C5–C4	122.47(13)
N3–Cu1–N1	81.18(5)	C2–C3–C4	120.08(13)
N4–Cu1–N1	159.85(5)	N4–C7–C6	111.94(11)
O5–Cu1–O1	174.70(4)	N6–C12–N5	117.20(12)
N3–Cu1–O5	84.17(5)	C6–C8–C9	111.09(12)
N4–Cu1–O2	95.66(5)	N4–C7–C10	123.93(12)
N1–Cu1–O5	83.81(5)	N1–C5–N2	116.74(12)
C1–N1–Cu1	128.84(9)	N3–C6–C8	124.01(12)
O3–Cl1–O1	109.07(7)	O4–Cl1–O1	109.18(7)
C5–N1–Cu1	112.21(9)	C12–O5–Cu1	122.57(7)

#1 -x, -y+2, -z+1; #2 -x+3/2, -y+1, -z

Table3

Hydrogen bonds (Å and °)

D–H···A	*d*(D–H)	*d*(H···A)	*d*(D···A)	∠(D–H–A)	Symmetry code
For **L^1H_2**					
C7–H7A...N1#2	0.96	2.64	3.356(2)	132.0	-x, y+1/2, -z+1/2
N2–H2A...N1#2	0.86	2.63	3.4531(19)	159.9	-x, y+1/2, -z+1/2
For **L^2H_2**					
N2–H2...N3#2	0.86	2.45	3.2176(18)	148.2	-x+1, y, -z+1/2
For **2**					
O9–H9E...O1#1	0.82	2.21	3.0219(17)	170.5	-x+1, y+1/2,-z+1/2

O9–H9D...O3	0.82	2.19	2.9969(18)	168.0	
C16–H16...O2#1	0.95	2.49	3.3370(18)	148.9	-x+1,y+1/2,-z+1/2
C8–H8A...O6#2	0.99	2.52	3.355(2)	141.4	-x+1,-y+1,-z+1
C1–H1...O2#1	0.95	2.46	3.3561(18)	156.5	-x+1,y+1/2,-z+1/2
N5–H5...O9#3	0.88	1.96	2.8231(16)	164.9	-x+2,y-1/2,-z+1/2
N2–H2...O6#2	0.88	2.00	2.8700(17)	169.1	-x+1,-y+1,-z+1

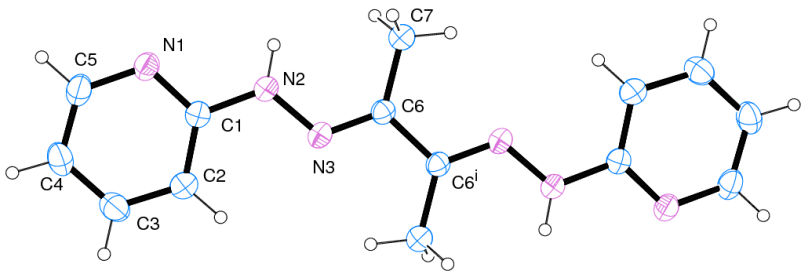

Fig. 1. ORTEP of $\mathbf{L^1H_2}$ with 30% probability ellipsoids. Symmetry code i) -x, -y+2, -z+1

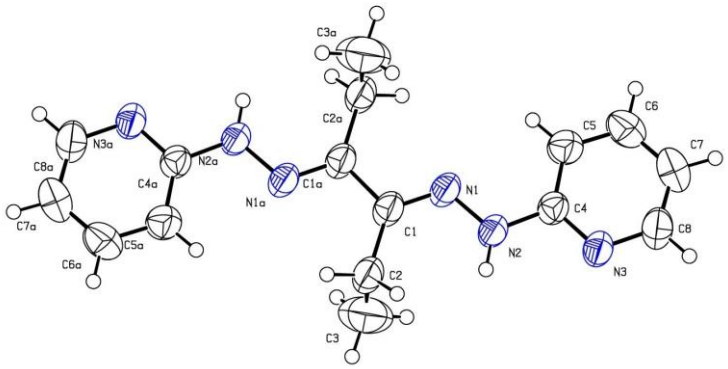

Fig. 2. ORTEP of $\mathbf{L^2H_2}$ with 30% probability ellipsoids. Symmetry code i) -x+3/2, -y+1, -z

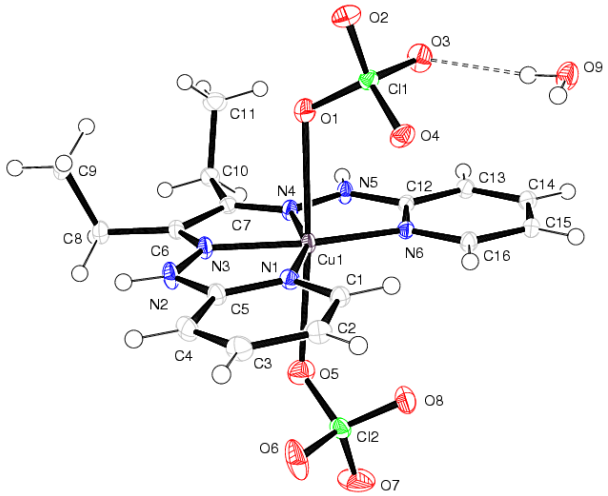

Fig. 3. ORTEP of **2** with 30% probability ellipsoids

3.3. HSA binding study

3.3.1. Absorption spectroscopic study

Fig. 4 shows the absorption spectra of $\mathbf{L^1H_2}$ and $\mathbf{L^2H_2}$ and their complexes in aqueous and protein (HSA) environments. It is evident that the absorption of both the ligands decreases upon addition of HSA; while the reverse is true for their complexes. The perturbation in absorption in presence of HSA was more pronounced in case of the complexes. The UV data were used to construct the Benesi-Hilderbrand plot for 1:1 complexation using the following equation:

$$\frac{1}{\Delta A} = \frac{1}{\Delta A_{\max}} + \frac{1}{K\Delta A_{\max}[HSA]} \qquad (5)$$

Here, $\Delta A = |A_x - A_0|$ and $\Delta A_{max} = |A_\infty - A_0|$, where A_0, A_x and A_∞ are the absorbances of the ligand or complex in the absence of HSA, at an intermediate HSA concentration, and at a concentration of complete interaction with HSA respectively. K is the association constant and [HSA] is the protein concentration. A plot of $\Delta A_{max}/\Delta A$ would give a straight line with the intercept of 1 and the slope 1/[HSA]. The inverse of slope would yield the association constant. The association constants were found to be 2.16±0.18 × 10^4 M^{-1} and 3.78±0.29 ×

10^4 M^{-1} for $\mathbf{L^1H_2}$ and $\mathbf{L^2H_2}$ respectively. For **1** and **2**, it was found respectively to be 6.36±0.47 × 10^4 M^{-1} and 8.25±0.55 × 10^4 M^{-1}. These results clearly demonstrate the stronger binding ability of the metal complexes with HSA compared to their ligand counterparts.

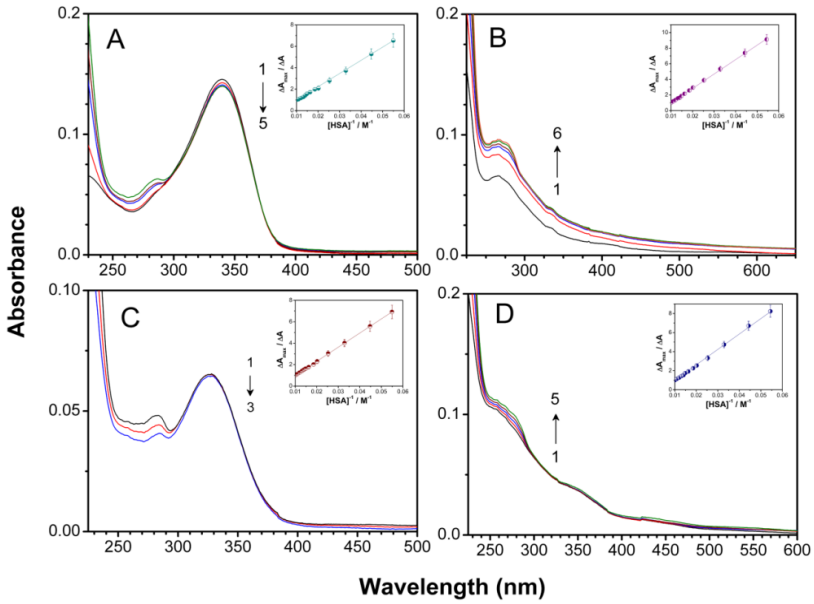

Fig. 4. Absorbance titration profiles of $\mathbf{L^1H_2}$, $\mathbf{L^2H_2}$, **1** and **2** with increasing concentration of HSA. **Panel A**: Curve 1-5 represents absorption spectra of free $\mathbf{L^1H_2}$ (4.9 μM, curve 1) treated with 6.34, 12.66, 25.32 and 42.2 μM of HSA; **Panel B**: Curve 1-6 represents absorption spectra of free **1** (4.9 μM, curve 1) treated with 1.58, 3.17, 6.34, 12.66 and 25.32 μM of HSA; **Panel C**: Curve 1-3 represents absorption spectra of free $\mathbf{L^2H_2}$ (4.9 μM, curve 1) treated with 25.32 and 42.2 μM of HSA; **Panel D**: Curve 1-5 represents absorption spectra of free **2** (4.9 μM, curve 1) treated with 3.17, 6.34, 12.66, 25.32 and 42.2 μM of HSA. Inset of each figure shows the respective Benesi-Hilderbrand plot.

3.3.2. Fluorescence spectroscopic studies

Addition of HSA results in small changes in the absorption spectra of the systems. Now, since all the systems are fluorescence inactive itself, here fluorescence titrations were carried out by titrating HSA with increasing concentration of ligand/complex. Interestingly, HSA induced changes in the fluorescence spectra of the systems (spectral shift or intensity

distribution) are much more pronounced. This is evident from some of the representative spectra shown in Fig. 5. Significant red shift as well as enhancement in emission intensity is observed in all cases, though the extent of enhancement is more pronounced in case of the complexes. Benesi-Hilderbrand plots (not shown) were constructed for all the cases. The association constants were found to be 2.02±0.15 × 10^4 and 3.51±0.24 × 10^4 M^{-1} for $\mathbf{L^1H_2}$ and $\mathbf{L^2H_2}$ respectively. For **1** and **2**, those were found respectively to be 6.21±0.42 × 10^4 and 8.01±0.53 × 10^4 M^{-1}. Thus, the fluorescence spectral data are found to be in good agreement with the absorption results.

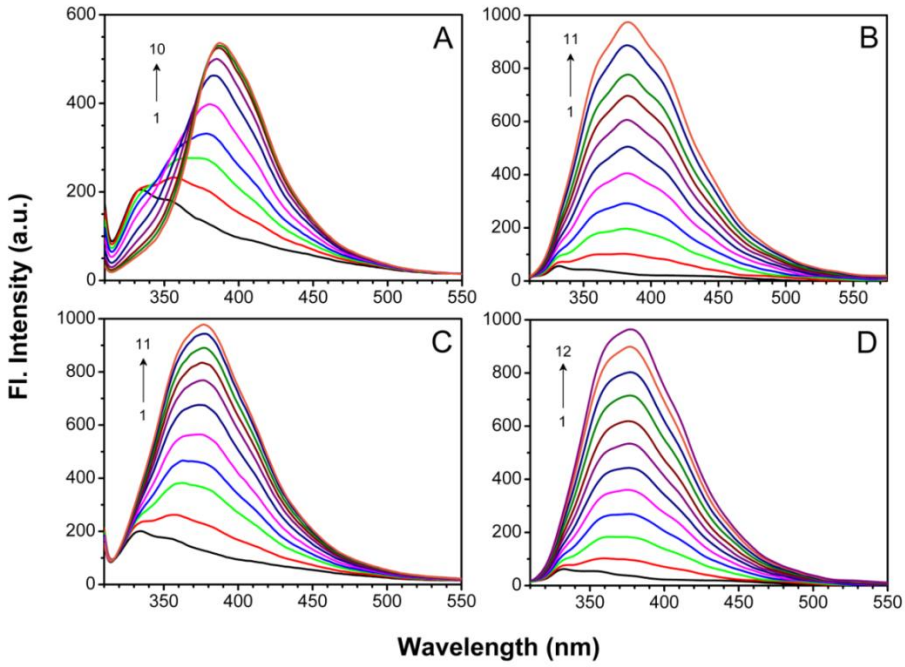

Fig. 5. Emission spectra of $\mathbf{L^1H_2}$, $\mathbf{L^2H_2}$, **1** and **2** with increasing concentration of HSA. **Panel A:** Fluorescence spectra of free $\mathbf{L^1H_2}$ (9.2 μM, curve 1) treated with 1.56, 3.13, 4.69, 6.24, 7.79, 12.43, 18.58, 30.72 and 48.58 μM of HSA; **Panel B:** Fluorescence spectra of free **1** (9.2 μM, curve 1) treated with 0.78, 1.56, 3.13, 4.69, 6.24, 7.79, 10.89, 15.51, 21.63 and 30.72 μM of HSA; **Panel C:** Fluorescence spectra of free $\mathbf{L^2H_2}$ (9.2 μM, curve 1) treated with 1.56, 3.13, 4.69, 6.24, 7.79, 12.43, 18.58, 24.67, 30.72 and 44.16 μM of HSA; **Panel D:** Fluorescence spectra of free **2** (9.2 μM, curve 1) treated with 0.78, 1.56, 3.13, 4.69, 6.24,

7.79, 9.34, 12.43, 18.58, 24.68 and 30.72 μM of HSA in 10 mM CP buffer of pH 7.0 at 25 °C.

The tryptophan residue of HSA shows a strong fluorescence emission with a peak at 338 nm when its excitation is performed at 280 nm. In Fig. 5, it is not clearly visible since the current profile depicts the titration where the emission intensity increases abruptly. Consequently, this emission has been obscured in the envelope of the final spectrum. The spectrum of native HSA has been shown in Fig. 6.

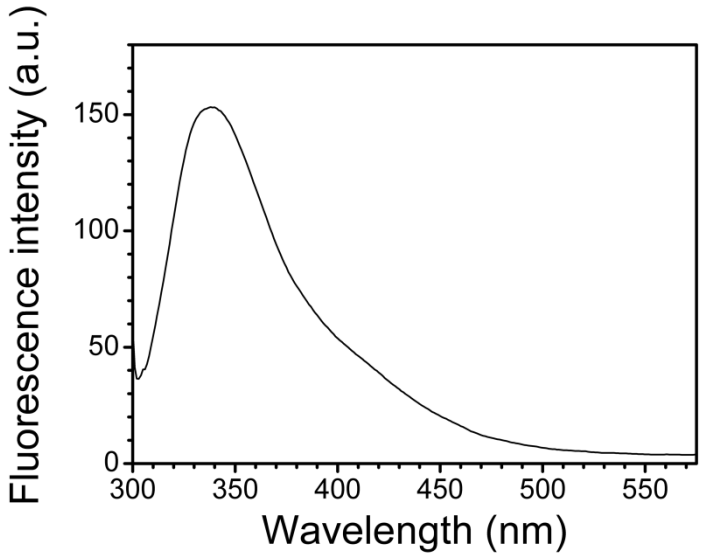

Fig. 6. Fluorescence spectrum of free HSA in 10 mM CP buffer of pH 7.0 at 25 °C.

The spectrum clearly manifests a maximum around 338 nm. According to Lakowicz [25], fluorescence spectra of protein in presence of small molecules undergo changes due to a good number of phenomenon like excited state reactions, molecular rearrangements, energy transfer, ground state complexation, collision quenching etc. Probably, the excited state energy transfer is taking place between the tryptophan residue and the ligands as well as metal complexes. Several examples are known in the literature where the metal complexes even give rise to quenching of fluorescence emission on binding to HSA [26,27]. However, mere residing near the Trp residue does not always result in quenching. Recently, Dey et al has shown that the emission of albumin proteins increases significantly in presence of some

carbazole containing probes [28]. In our present case, the observed enhancement in fluorescence intensity owing to HSA binding of the ligands as well as their complexes is most likely due to the concomitant change in microenvironment around Trp residues [28]. Our molecular docking study further reveals that the HSA binding occurs preferentially near Trp residue.

3.3.3. Fluorescence lifetime studies

Fluorescence lifetime measurement of the ligands as well as their complexes in presence of HSA was performed by using TCSPC technique. Fluorescence decay profiles are represented in Fig. 7. Fluorescence lifetime measurement often serves as an indicator of the local environment of a fluorophore and its response towards excited state interactions. Lifetime data obtained from the best fittings of the decay profiles and goodness of fits has been established from the χ^2 criterion (χ^2 will be within 0.95-1.05). The nature of decay of all these systems was bi-exponential in nature and remained the same in presence of HSA. The lifetime value was increased upon addition of HSA and the enhancement was more pronounced in case of the complexes compared to their respective ligand counterparts. Enhancement in the lifetime value is an indication of strong binding of the small molecule to the polynucleotide [29].

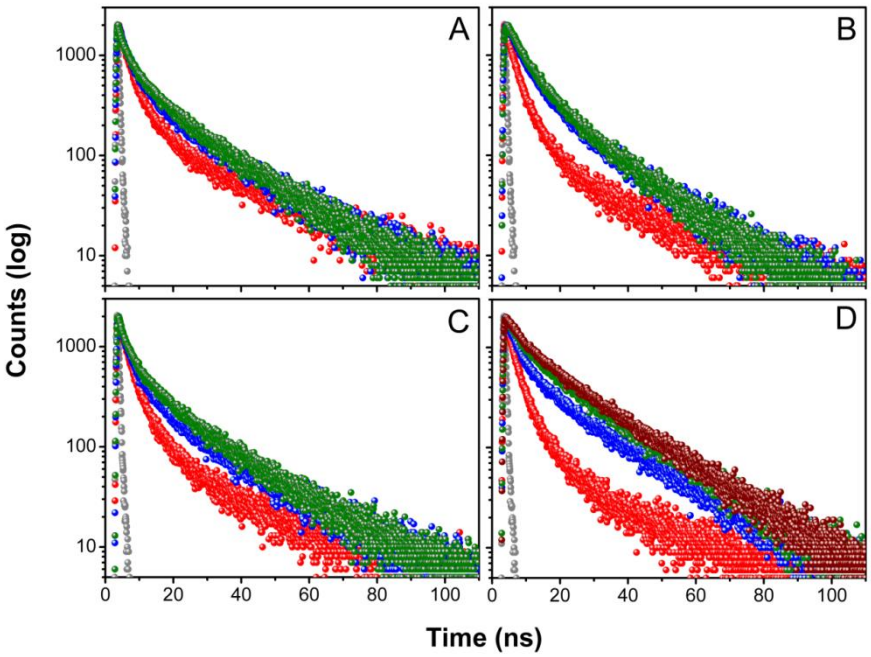

Fig. 7. Time-resolved fluorescence decay profile of $\mathbf{L^1H_2}$, $\mathbf{L^2H_2}$, **1** and **2** with increasing concentration of HSA. **Panel A**: decay profile of free $\mathbf{L^1H_2}$ (9.2 μM,●) treated with 12.66 μM (●) and 42.2 μM (●) of HSA; **Panel B**: decay profile of free **1** (9.2 μM,●) treated with 6.34 μM (●), 25.32 μM (●) of HSA; **Panel C**: decay profile of free $\mathbf{L^2H_2}$ (9.2 μM,●) treated with 12.66 μM (●) and 42.2 μM (●) of HSA; **Panel D**: decay profile of free **2** (9.2 μM,●) treated with 3.17 μM (●), 6.34 μM (●) and 25.32 μM (●) of HSA in 10 mM CP buffer of pH 7.0 at 25 °C.

3.3.4. Thermodynamics of the interaction

Thermodynamic parameters for the association of present ligands and their copper(II) complexes were calculated from the temperature dependent binding constants using fluorescence spectroscopic studies in 10 mM CP buffer of pH 7.0. The values of the thermodynamic parameters are tabulated in Table 4. The van't Hoff plot for binding of $\mathbf{L^1H_2}$ with HSA is shown in Fig. 8.

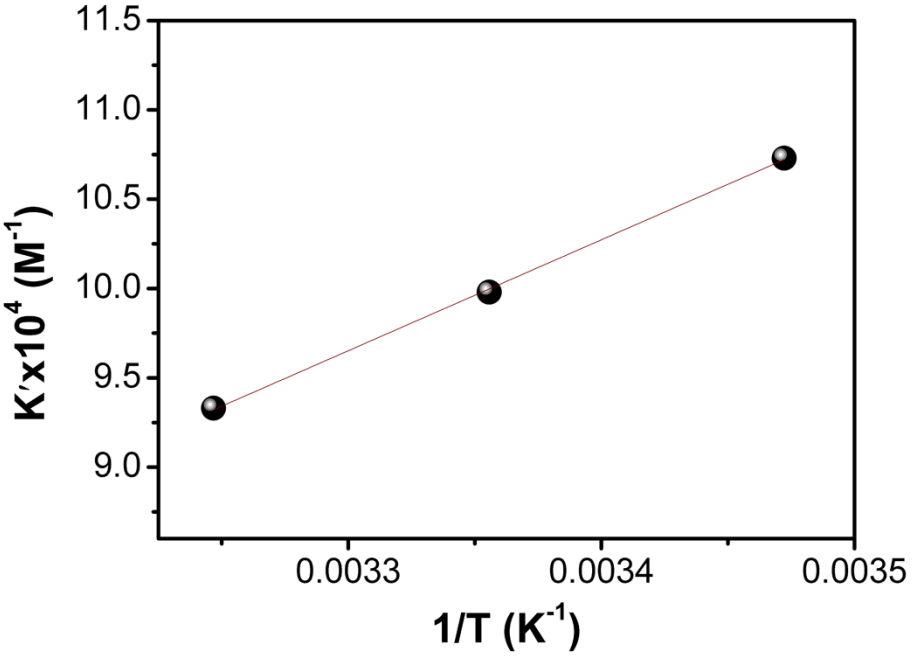

Fig. 8. van't Hoff plot for binding of $\mathbf{L^1H_2}$ with HSA

Linear fit of the data indicates a very small value of heat capacity change ($\Delta C_P \approx 0$). It can be seen that in each case the binding was characterized by both negative enthalpy and entropy changes.

Table4

Thermodynamic parameters for the interaction of ligands and complexes with HSA in 10 mM CP buffer, pH 7.0 obtained from fluorescence spectrophotometry.[a]

Sample	Temperature (in K)	K´ x 10^4 M^{-1}	ΔG° (kJ mol^{-1}) at 25 ºC	ΔH°(kJ mol^{-1}) at 25 ºC	TΔS° (kJ mol^{-1}) at 25 ºC
$\mathbf{L^1H_2}$	**288**	**4.67**±0.28	-24.78±1.04	-51.64±1.93	-26.86±1.21
	298	**2.02**±0.15			
	308	**1.10**±0.09			
1	**288**	**11.92**±0.58	-27.40±1.25	-53.11±2.01	-25.71±1.09
	298	**6.21**±0.42			

	308	**3.01**±0.21			
	288	7.01±0.48			
L^2H_2	**298**	3.51±0.24	-26.11±1.14	-51.89±1.95	-25.78±1.11
	308	1.63±0.13			
	288	**15.83**±0.72			
2	**298**	**8.01**±0.53	-28.05±1.29	-53.76±2.03	-25.71±1.09
	308	**3.74**±0.25			

a Average of three determinations

Our thermodynamic data revealed that the binding process was facilitated by negative enthalpy change and was opposed by negative entropy change. The negative enthalpy change for the binding process may be explained in the spirit of van der Waals' stacking interactions [11,30], hydrophobic as well as weak electrostatic interactions. Negative entropy change for the interaction process may be attributed to the increase in order of the formation of rigid complex.

3.4. Molecular docking study

We have docked 4 systems into the 3D structure of HSA using AutoDock Tools. These models provide the most probable binding sites and poses in the protein that have not resulted in structural alteration of HSA. The location of the fluorescence active Trp-214 moiety of HSA is shown in Fig. 9. Trp-214 moiety resides in domain II of HSA. From Fig. 9, it is obvious that all the systems reside near the Trp residue. As a result, so much perturbation of fluorescence spectra of HSA has been observed in presence of all the systems. It is a point to note that the difference in anchoring position between the ligands and their complexes was not so significant. Here, molecular docking study was undertaken only to show the probable location of binding of the ligands and their complexes.

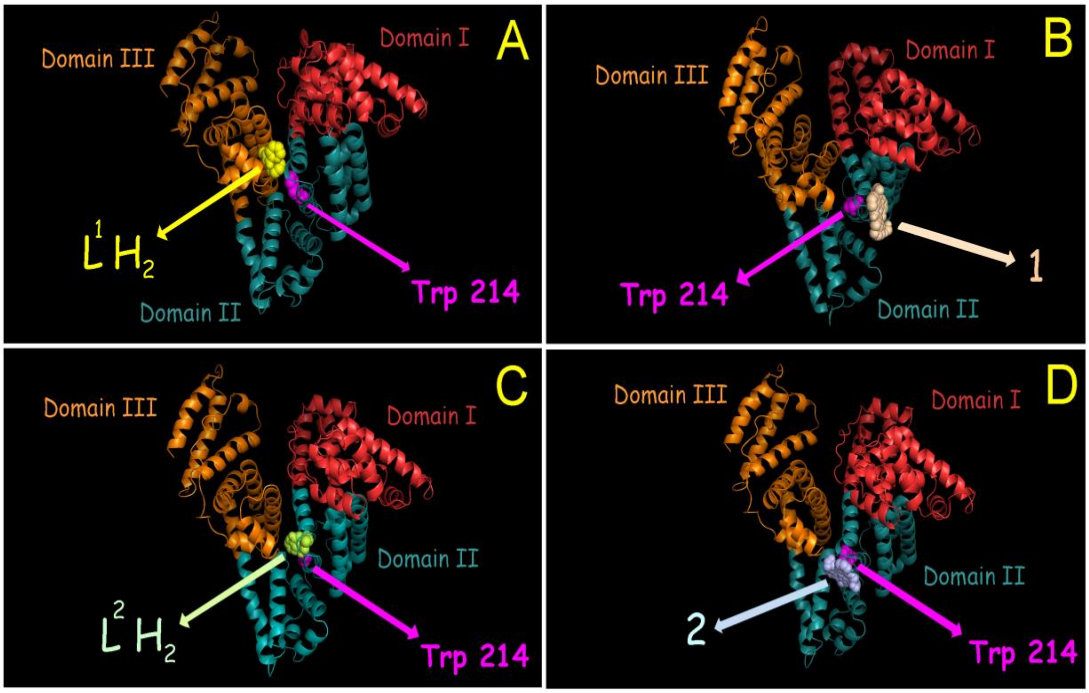

Fig. 9. Stereo view of the docked conformation of the systems with HSA in near vicinity (4 Å).

For copper(II) complexes, HSA offers two specific binding sites — the N-terminal site (NTS) and the multi-metal binding site (MBS) [31]. The NTS strongly binds Cu(II) ions preferentially over the MBS. This NTS comprises Asp-Ala-His, the first three amino acid residues of the HSA sequence [31]. Employing nitrilotriacetic acid (NTA) as a low molecular weight competitor, Rózga et al had earlier demonstrated experimentally through competitive spectroscopic evaluation of conditional stability constant that the HSA binds copper(II) ions at the NTS of HSA. From this study it is apparent that the conditional stability of a copper(II) system is crucial for its binding at the NTS of HSA. To augment our present situation, we have taken recourse to check the stability of $\mathbf{L^1H_2}$, $\mathbf{L^2H_2}$, **1** and **2** through absorption spectrophotometric means maintaining the physiological pH under the same experimental conditions of our HSA binding studies. Our exercise prompts us to predict that the observed binding is most likely to the NTS of HSA.

4. Conclusions

In this work, a novel osazone type Schiff base ligand, hexane-3,4-dione bis(2′-pyridylhydrazone) and its monomeric copper(II) complex have been synthesized and characterised through the available spectroscopic and analytical means. The X-ray crystal structures of them have also been determined. The X-ray crystal structure of an analogous ligand system, butane-2,3-dione bis(2′-pyridylhydrazone), has also been provided. Our spectroscopic investigations reveal that these ligands and their Cu(II) complexes bind to HSA, an important highly stable yet flexible blood plasma protein having 3D structure. Thermodynamic parameters for the interaction of ligands and their complexes with HSA have also been determined. Molecular docking studies also corroborate the binding of HSA with them.

Acknowledgements

Financial support received from the Science & Engineering Research Board (SERB), DST, New Delhi, Govt. of India under its Empowerment and Equity Opportunities for Excellence in Science Scheme (F. No. SB/EMEQ-029/2013) is humbly acknowledged. M.L.Z and L.P.L. appreciated the NSFC (Grant Nos. 21171109, 21271121 & 21571118), SRFDP (Grant Nos. 20111401110002 & 20121401110005), the Natural Science Foundation of Shanxi Province of China (Grant Nos. 2010011011-2 & 2011011009-1) and the Shanxi Scholarship Council of China (2012-004). We are thankful to the reviewers for their valuable suggestions. Thanks are also due to Prof. Nitin Chattopadhyay, Department of Chemistry, Physical Chemistry Section, Jadavpur University for various help.

References

[1] B. Chiswell, F. Lions, Quadridentate Chelate compounds. IV. metal complexes from butane-2,3-dione bis(2'-pyridylhydrazone), Inorg. Chem. 3 (1964) 490-492.

[2] B. Chiswell, F. Lions, M.L. Tomlinson, Tridentate chelate compounds. IV. metal complexes from α-diketone mono-α-pyridylhydrazone type ligands, Inorg. Chem. 3 (1964) 492-499.

[3] A.A. Schilt, J.F. Wu, F.H. Case, Synthesis and metallochromic properties of some new mono- and bishydrazones of benzil and 2,2'-pyridyl, Talanta 22 (1975) 915-917.

[4] M.M. Rodriguez, A.G. Asuero, Studies on pyridylhydrazones derived from biacetyl as analytical reagents [1], Microchem J. 25 (1980) 309-322.

[5] A.G. Asuero, Preliminary evaluation of biacetyl bis(2-Pyridyl)hydrazone as an analytical reagent, Microchem J. 23 (1978) 390-399.

[6] B. Guhathakurta, C. Biswas, J.P. Naskar, L. Lu ,M. Zhu, Synthesis and crystal of [Cu(BDBPH)(ClO_4)$_2$](BDBPH = butane-2,3-dione bis(2'-pyridylhydrazone), J. Chem. Crystallogr. 41 (2011) 1694-1699.

[7] R.J. Olcott, R.H. Holm, The crystal and molecular structure of the electron transfer complex butane-2, 3-dione-bis(2′-pyridyl-hydrazonato)nickel, [Ni(BDPH)-2H], Inorg. Chim. Acta 3 (1969) 431-437.

[8] A.R. Timerbaev , C.G. Hartinger , S.S. Aleksenko , B.K. Keppler, Interactions of antitumor metallodrugs with serum proteins: advances in characterization using modern analytical methodology, Chem. Rev. 106 (2006) 2224–2248.

[9] U. Kragh-Hansen, Molecular aspects of ligand binding to serum albumin, J. Pharmacol. Rev. 33 (1981) 17-53.

[10] F. Faridbod, M.R. Ganjali, B. Larijani, S. Riahi, A.A. Saboury, M. Hosseini, P. Norouzi, C. Pillip, Interaction study of pioglitazone with albumin by fluorescence spectroscopy and molecular docking, Spectrochim. Acta Part A 78 (2011) 96–101.

[11] X.-B. Fu, G.-T. Weng, D.-D. Liu, X.-Y. Le, Synthesis, characterization, DNA binding and cleavage, HSA interaction and cytotoxicity of a new copper(II) complex derived from 2-(2′-pyridyl)benzothiazole and glycylglycine, J. Photochem. Photobiol. A: Chem. 276 (2014) 83–95.

[12] M.-Y. Tian, X.-F. Zhang, L. Xie, J.-F. Xiang, Y.-L. Tang, C.-Q. Zhao, The effect of Cu^{2+} on the interaction between an antitumor drug-mitoxantrone and human serum albumin, J. Mol. Struct. 892 (2008) 20–24.

[13] A. Massey, Y.-Z. Xu, P. Karran, Photoactivation of DNA thiobases as a potential novel therapeutic option, Curr. Biol. 11 (2001) 1142–1146.

[14] N. Bandyopadhyay, M. Zhu, L. Lu, D. Mitra, M. Das, P. Das, A. Samanta, J.P. Naskar, Synthesis, structure, spectral characterization, electrochemistry and evaluation of antibacterial potentiality of a novel oxime-based palladium(II) compound, Eur. J. Med. Chem. 89 (2015) 59–66.

[15] G. Tamasi, F. Serinelli, M. Consumi, A. Magnani, M. Casolaro, R. Cini, Release studies from smart hydrogels as carriers for piroxicam and copper(II)-oxicam complexes as anti-inflammatory and anti-cancer drugs. X-ray structures of new copper(II)-piroxicam and -isoxicam complex molecules, J. Inorg. Biochem. 102 (2008) 1862–1873.

[16] B.N. Ames, M.K. Shigenaga, T.M. Hagen, Oxidants, antioxidants, and the degenerative diseases of aging, Proc. Natl. Acad. Sci. USA 90 (1993) 7915–7922.

[17] W.C. Wolsey, Perchlorate salts, their uses and alternatives, J. Chem. Educ. 50 (1973) A335.

[18] B.P. Espbósito, A Faljoni-Alhio, J.F.S. Menezes, H.F. Brito, R. Najjar, A circular dichroism and fluorescence quenching study of the interactions between rhodium(II) complexes and human serum albumin, J. Inorg. Biochem. 75 (1999) 55-61.

[19] Bruker, SMART (Version 5.0) and SAINT (Version 6.02). Bruker AXS Inc., Madison, Wisconsin, USA, 2000.

[20] G.M. Sheldrick, SADABS, University of Gottingen, Germany, 2000.

[21] G.M. Sheldrick, SHELXS97 and SHELXL97, University of Gottingen, Germany, 1997.

[22] N. Bandyopadhyay, A.B. Pradhan, S. Das, L. Lu, M. Zhu, S. Chowdhury, J.P. Naskar, Synthesis, structure, DFT calculations, electrochemistry, fluorescence, DNA binding and molecular docking aspects of a novel oxime based ligand and its palladium(II) complex, J. Photochem. Photobiol. B Biol. 160 (2016) 336–346.

[23] Y. Fukuda, A. Shimura, M. Mukaida, E. Fujita, K. Sone, Studies on mixed chelates-III mixed copper(II) chelates with N,N,N',N'-tetramethylethylenediamine and β-diketones[1], J. Inorg. Nucl. Chem. 36 (1974) 1265-1270.

[24] A. Sengul, I. Yilmaz, E. Sahin, N. Karadayi, Spectroscopic and structural studies of 6,6′- bis(N-methylhydrazine)-2,2′-bipyridine and its mononuclear copper(II) complex, J. Coord. Chem. 63 (2010) 3453–3462.

[25] J. R. Lakowicz, Principles of Fluorescence Spectroscopy, Plenum Press: New York, 2006.

[26] S.-S. Wu, W.-B. Yuan , H.-Y. Wang, Q. Zhang, M. Liu, K.-B. Yu, Synthesis, crystal structure and interaction with DNA and HSA of (N,N′-dibenzylethane-1,2-diamine) transition metal complexes, J. Inorg. Biochem. 102 (2008) 2026-2034.

[27] Q. Gan, X. Fu, W. Chen, Y. Xiong, Y. Fu, S. Chen, X. Le, Synthesis, DNA/HSA Interaction Spectroscopic Studies and In Vitro Cytotoxicity of a New Mixed Ligand Cu(II) Complex, J. Fluoresc. 26 (2016) 905-918.

[28] G. Dey, P. Gaur, R. Giri, S. Ghosh, Optical signaling in biofluids: a nondenaturing photostable molecular probe for serum albumins, Chem. Commun. 52 (2016) 1887-1890.

[29] S. Das, S. Parveen, A.B. Pradhan, An insight into the interaction of phenanthridine dyes with polyriboadenylic acid: Spectroscopic and thermodynamic approach, Spectrochim. Acta A 118 (2014) 356-366.

[30] X.-B. Fu, Z.-H. Lin, H.-F. Liu, X.-Y. Le, A new ternary copper(II) complex derived from 2-(2′-pyridyl)benzimidazole and glycylglycine: Synthesis, characterization, DNA binding and cleavage, antioxidation and HSA interaction, Spectrochim. Acta A 122 (2014) 22–33.

[31] M. Rózga, M. Sokołowska, A. M. Protas, W. Bal, Human serum albumin coordinates Cu(II) at its N-terminal binding site with 1 pM affinity, J. Biol. Inorg. Chem. 12 (2007) 913–918.

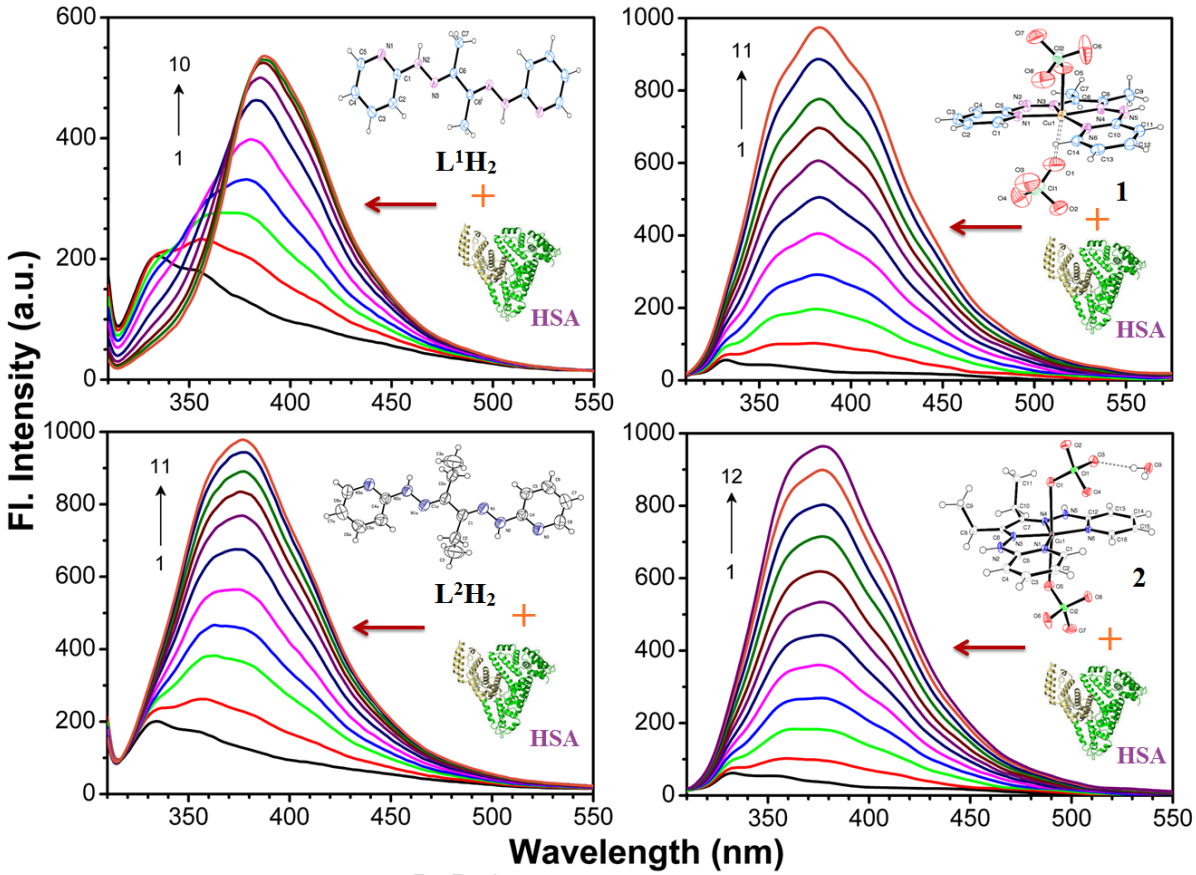

Graphical Abstract

Highlights

- Osazone based ligand and its copper(II) complex have been structurally characterized.
- Interactions of HSA with these compounds have been studied by various spectroscopic means.
- Thermodynamic parameters for the interaction have been determined.
- Molecular docking aspects have also been provided.